ELSEVIER

Thermochimica Acta 377 (2001) 9–33

thermochimica acta

www.elsevier.com/locate/tca

Measurement of heat capacity to gain information about time scales of molecular motion from pico to megaseconds☆

B. Wunderlich[a,b,*], M. Pyda[a,b], J. Pak[a,b], R. Androsch[c]

[a]*Department of Chemistry, The University of Tennessee, Knoxville, TN 37996-1600, USA*
[b]*Oak Ridge National Laboratory, Chemical and Analytical Sciences Division, Oak Ridge, TN 37831-6197, USA*
[c]*Institute of Material Science, Martin-Luther-University Halle-Wittenberg, Geusaer Str., 06217 Merseburg, Germany*

Received 11 August 2000; received in revised form 27 January 2001; accepted 1 February 2001

Abstract

Molecular motion has primarily a time scale of picoseconds. Quantum mechanical models of small-amplitude vibrations and local, large-amplitude motions can be fitted quantitatively to equilibrium heat capacities. Macroscopic calorimetry, thus yields indirectly the characteristic frequencies of molecular motion in the range of 10^{11}–10^{13} Hz. At lower temperature, much of the large-amplitude molecular motion is restricted to cooperative movements and slows to macroscopic times so that calorimetry can directly measure the kinetics of these changes which may extend the time scales to megaseconds and beyond. In this light, instrumentation and interpretation of differential scanning temperature-modulated calorimetry (DSTMC) are discussed. Six basic thermal effects govern the thermal analysis of linear macromolecules: (1) the vibrational heat capacity; (2) heat capacities arising from large amplitude molecular motion; (3) reversible transitions; (4) annealing; (5) secondary crystallization and (6) primary crystallization. Of these only (1)–(3) are reversible. To these six thermal effects that do not change the molecular integrity, chemical reactions, evaporation, and condensation have to be added for a full thermal analysis. The latter effects have not been treated in this paper. Published by Elsevier Science B.V.

Keywords: Temperature-modulated calorimetry; Heat capacity; Latent heat; Time scale; Reversibility

1. Introduction

Differential scanning temperature-modulated calorimetry (DSTMC) originated in the early 1990s [1–3] and has become by now an established technique of thermal analysis. Its development can be followed by the discussions held during the last four Lähnwitz seminars in 1994, 1996, 1998, and 2000. At the third seminar in 1994, we reported on ''Modulated DSC — Capabilities and Limits''. This lecture dealt with the early developments of temperature modulation of the standard differential scanning calorimetry (DSC). It was possible to describe the experimental basis and the data treatment for the conditions of steady state in the calorimeters and negligible temperature gradient within the sample [4,5]. The presentations of the fourth to the sixth seminars are published in collected volumes of *Thermochimica Acta* [6–8]. Our contributions consisted of the ''Heat Capacity Determination

☆ Presented at the sixth Lähnwitz seminar. This manuscript has been authored by a contractor of the US Government under the contract no. DOE-AC05-00OR22725. Accordingly, the US Government retains a non-exclusive, royalty-free license to publish or reproduce the published form of this contribution, or allow others to do so, for US Government purposes.

* Corresponding author. Tel.: +1-865-974-0652; fax: +1-865-974-3419.
E-mail address: athas@utk.edu (B. Wunderlich).

0040-6031/01/$ – see front matter. Published by Elsevier Science B.V.
PII: S0040-6031(01)00539-1

by Temperature-Modulated DSC and its Separation from Transition Effects'' [9], the ''Temperature-Modulated Differential Scanning Calorimetry of Reversible and Irreversible First-Order Transitions'' [10]. In the fourth seminar, the discussion centered about the methods of heat-capacity measurement and the special problems that arise from the glass transition. Even without an enthalpy of transition, deviations from linearity were observed for the apparent heat capacity in the glass transition region and could be linked quantitatively to the kinetic parameters of the process [11–14]. Also, at the fourth Lähnwitz seminar [9], a new observation was reported: quasi-isothermal DSTMC (differential scanning temperature-modulated calorimetry, also called TMDSC or MTDSC by permutation of the description of the technique), revealed a small, reversing contribution to polymer melting [15–18]. This was surprising since flexible, linear macromolecules should melt irreversibly [19]. Based on the latter observations, detailed research on first-order transitions was begun and the results were presented at the fifth Lähnwitz seminar [10]. It involved the study of the first-order transitions of small and large molecules and is continuing to produce major new insight into the melting, crystallization, and annealing of polymers, as for example in copolymers of ethylene and 1-octene [20,21]. Our research topic for the last 2 years was the simultaneous modulation with several frequencies, a topic that became evident when it could be shown during the fifth Lähnwitz seminar how the loss of steady state in sawtooth modulation could be handled for data analysis [10]. The development of this topic led to the invention of complex sawtooth modulation [22], which can be generated even with a standard DSC, and was tested in heat-flux calorimeters with modulations that were controlled at the position at the sample [23] or the heater [24] and in power-compensation calorimeters [25]. The results of this study permitted not only the analysis of time-dependent processes in a single experiment, but also eliminated the need for a negligible temperature gradient within the sample by means of an internal calibration, as is detailed in Section 4.

Performing calorimetry while the sample temperature undergoes periodic oscillations, one adds time or frequency as parameters to the measurement, i.e. one may quantitatively study not only classical equilibrium systems, but also non-equilibrium states and their approach to thermodynamic equilibrium. The purpose of this paper is to elucidate the various time scales of importance to classical and time-dependent calorimetry. Today, one knows that the molecular motions are the ultimate time-dependent processes in materials and it is easy to represent the atomic motion by molecular dynamics simulations using supercomputers [26]. It is thus attempted in this paper to discuss the means to connect calorimetry directly to molecular motion which ultimately may lead to ''Thermal Analysis via Molecular Dynamics Simulation'' [27]. It will be shown that it is important to handle time scales from picoseconds to megaseconds (10^{-12} to 10^{6} s), where a megasecond covers a measuring time of about 2 weeks. The fastest processes are described by fitting quantum-mechanical models to the temperature dependence of the equilibrium heat capacity (Sections 2 and 3) and the slower ones can be measured directly (Section 5).

2. Heat capacity due to vibrational molecular motion

Heat capacity, C_p, is the heat needed to increase the temperature of the system in question by 1 K written as $\partial(H/\partial T) = C_p$, at constant pressure and number of moles.[1] It is the basic quantity derived from DSC experiments from the heat-flow rate, Φ (often also written as HF, which is proportional to $\Delta T = T_r - T_s$, the difference between reference and sample temperatures). A recent summary of heat capacity is given in [28]. The interpretation of these heat capacities has led to the ATHAS Data Bank [29]. In DSTMC, C_p can be derived from either the underlying heat-flow rate $\langle\Phi\rangle$ and the corresponding underlying rate of temperature change $\langle\dot{T}_s\rangle$ as a total C_p, or from the modulation amplitudes of T_s and Φ as reversing C_p, as will be discussed in more detail in Section 4.

The connection between the macroscopic internal energy and the microscopic molecular motion is most easily established for solids. At sufficiently low temperature only vibrational motion is possible. The

[1] For more details, see the 36 lectures of the computer course on Thermal Analysis of Materials, downloadable from the Internet: http://web.utk.edu/~athas/courses/tham99.html.

classical model of motion in solids is to assume that each atom can carry out vibrations in the three dimensions of space. Such motion should contribute a heat capacity at constant volume of $C_v = 3R$ J K^{-1} mol^{-1}, where R is the gas constant (8.314 J K^{-1} mol^{-1}) and $C_v = (\partial U/\partial T)$ at constant pressure and volume (where U is the internal energy). Indeed, this was observed to be true for many metals at not too low temperature (Dulong–Petit's rule [30]) and served in the 19th century to establish molar masses by measurement of heat capacity.

When approaching the zero of temperature, the heat capacity for all solids approaches zero. This experimental fact became one of the basic supports of the quantum mechanical description of molecular motion. Einstein [31] could show that assuming all vibrations in a monatomic solid have the same frequency, the quantum mechanical description of this vibration would lead to the observed decrease in heat capacity. This characteristic frequency is called the Einstein frequency and given in terms of the Einstein temperature Θ_E (in K) $= h\nu/k = 4.8 \times 10^{-11}\nu$, where ν is the frequency in Hz, and Θ_E expresses also the temperature at which the heat capacity reaches 92% of its classical value R. Typical values of Θ_E are 150 K ($\nu = 3 \times 10^{12}$ Hz) for Na and 385 K ($\nu = 8 \times 10^{12}$ Hz) for Al. For diamond, a much harder crystal with stronger bonds between the atoms, Θ_E is 1450 K ($\nu = 3 \times 10^{13}$ Hz), i.e. at room temperature, the Dulong–Petit rule holds for Na, less well for Al, and not at all for diamond. These Einstein frequencies allow a first link of heat capacity to the time scale of its cause, the vibrational motion. The order of magnitude of the time scale is the picosecond, 10^{-12} s.

Vibrational motion in solids, however, is not a single frequency. The vibrations are coupled and produce a vibrational spectrum which reaches to the acoustic frequency range. A common model to account for the frequency distribution was derived by Debye for an isotropic, three-dimensional solid [32]. It results in a quadratic distribution of the density of vibrational states, starting with zero vibrations at zero frequency and extending up to the Debye frequency Θ_D, which is fixed at the point where the number of vibrators has reached the maximum number of possible degrees of freedom ($=3N$, where N is the number of atoms). For diamond Θ_D is 2050 K ($\nu = 4.3 \times 10^{13}$ Hz).

At low temperatures, the Debye model works well for all crystals and leads to the well-known T^3 law of the temperature dependence of the heat capacity. For crystals with increasing anisotropy of bonding between the atoms, deviations occur already at quite low temperatures, and it is necessary to develop better approximations to the actual frequency spectrum, see for example [33]. For linear macromolecules, the degree of anisotropy is very high, and one must use more complex approximations [29]. Fig. 1 shows, as an example, the heat capacity of polyethylene, and its various contributions from the vibrational spectrum. It is obvious that the acoustic frequencies ($0–2 \times 10^4$ Hz) are negligible for the heat capacity, except for temperatures below 1.0 mK.

The skeletal vibrations for polyethylene in Fig. 1 are practically fully excited at room temperature, i.e. their heat capacity contribution assumes the classical value. The skeletal vibrations are mainly torsional and bending oscillations of the chain. The group vibrations are much higher in frequency and are similar for the same chemical grouping of atoms in different molecules. In polyethylene, they consist of the C–C-stretching and the C–H-stretching and bending vibrations. Next, the change from C_v to C_p can be calculated from the expansivity and the compressibility, or approximated based on the Nernst–Lindemann equation [34] as adapted to polymers [35].

Up to 300 K, the computed and experimental heat capacities agree well. For the contributions from the group vibrations no calorimetric measurements are necessary since the frequencies are known with high accuracy from normal mode calculations based on force constants extracted by fitting of the corresponding frequencies to infrared and Raman spectra. The skeletal contributions, in turn, can at present only be represented by fitting of the experimental, skeletal heat capacities to one- and three-dimensional Debye functions of frequencies Θ_1 and Θ_3, respectively, as outlined in [28]. For the heat capacity of a polymer crystal that exhibits only vibrational motion, thus one needs to derive only these two constants from calorimetry. Fig. 2 illustrates such an evaluation of Θ_1 and Θ_3 from the measurement of the heat capacity of chymotrypsinogen at low temperature. The unique minimum indicates that only one combination of Θ_1 and Θ_3 gives a fit within the error of the measurement, assuring the usefulness of the model. Glassy and

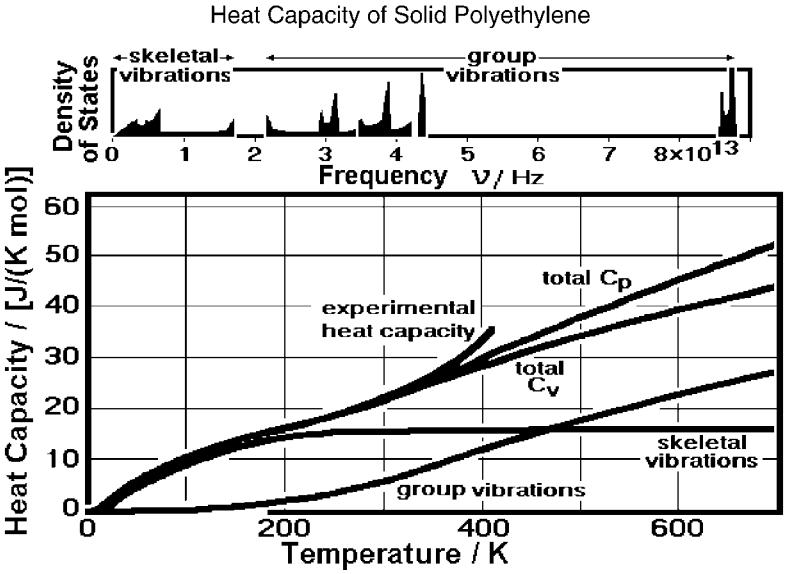

Fig. 1. Contributions of different types of vibrations to the heat capacity of crystalline polyethylene and the corresponding densities of vibrational states.

mesophase polymers can similarly be represented. Usually the value of Θ_1 of the disordered polymers is only little different from the Θ_1 of the crystal, while Θ_3 may be considerably smaller. For example, Θ_1 and Θ_3 for glassy polyethylene are 519 and 80 K ($\nu = 1.0 \times 10^{13}$ and 1.71×10^{12} Hz, respectively), while for crystalline polyethylene Θ_1 and Θ_3 are 519 and 158 K ($\nu = 1.0 \times 10^{13}$ and 3.3×10^{12} Hz, respectively).

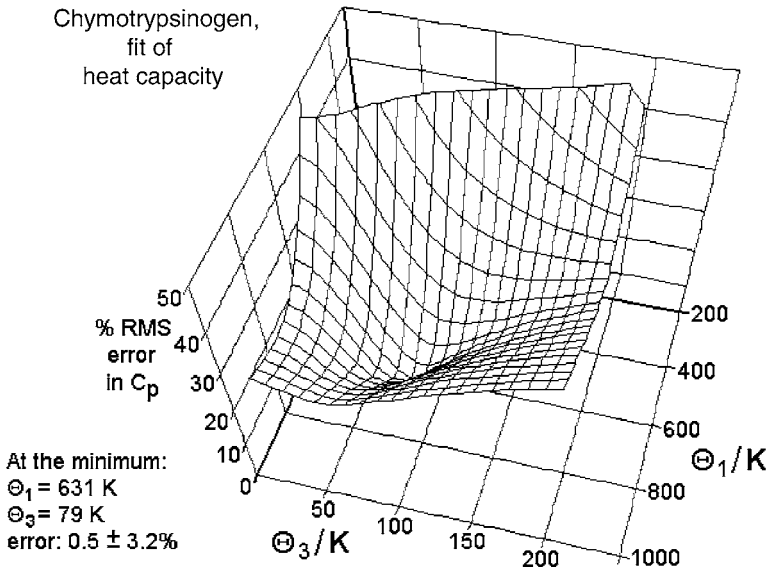

Fig. 2. Result of the fitting of the experimental, skeletal heat capacity of solid bovine α-chymotrypsinogen at low temperature (10–300 K). This protein has a molar mass of 25,646 Da and consists of 245 amino acids with a total of 3005 skeletal vibrations.

3. Heat capacity due to large-amplitude molecular motion

As the temperature of a crystal increases, some of the vibrations may change to a large-amplitude motion, i.e. to a translation, rotation, or internal rotation. Spherical molecules can only change three vibrational degrees of freedom into translations, each leading to a constant heat capacity of $0.5R\ \mathrm{J\ K^{-1}\ mol^{-1}}$. This causes a decrease in heat capacity if the potential energy decreases relative to that of the corresponding vibrators. A sufficiently asymmetric molecule may, in addition, change three vibrations into rotations with a similar decrease in heat capacity. Finally, flexible molecules may add internal rotations which are usually called conformational motions. At sufficiently high temperatures, all these changes reduce the heat capacity. At lower temperatures, large-amplitude motion causes usually an increase in the observed C_p since it involves positions of higher potential energy, such as gauche-to-*trans* conversions in polyethylene, and an increase in expansivity is needed to accommodate the large-amplitude motion. Fig. 3 illustrates this increase in heat capacity beyond the calculated vibrational limit for glassy polyethylene before it reaches the large increase due to the glass transition, and for crystalline polyethylene as it approaches the melting temperature.

To gain information on the details of motion, large-scale molecular-dynamics simulations were undertaken for polyethylene and compared to the experimental data [26]. Fig. 4 illustrates the distribution of torsional angles in the simulated crystalline polyethylene at 322 and 397 K. Clearly, besides the small-amplitude vibrations, a small number of large-amplitude rotations to the gauche-conformations occur in the crystal. Checking their lifetime, one finds that once created, they change back to the more stable *trans*-conformations within the order of magnitude of a picosecond. Comparing this short life time with the torsional vibrational frequency of about 3×10^{12} Hz, one must conclude that in this temperature range, for every 100 oscillations with a small amplitude, the *trans*-conformations flip once into a gauche-conformation. The connection of the simulation data to experiment is given in Fig. 5 [27], where the simulated gauche-conformations in paraffins are compared to measured concentrations from infrared experiments which can detect a specific vibration that is attributed to the gauche-conformation [36]. The deviation of the measured heat capacity from the vibrational heat capacity, shown in Fig. 3, is also in agreement with the number of the calculated gauche-conformations from the molecular-dynamics simulation [37].

The gauche-conformations within a crystal represent defects that govern the deformation of polymer

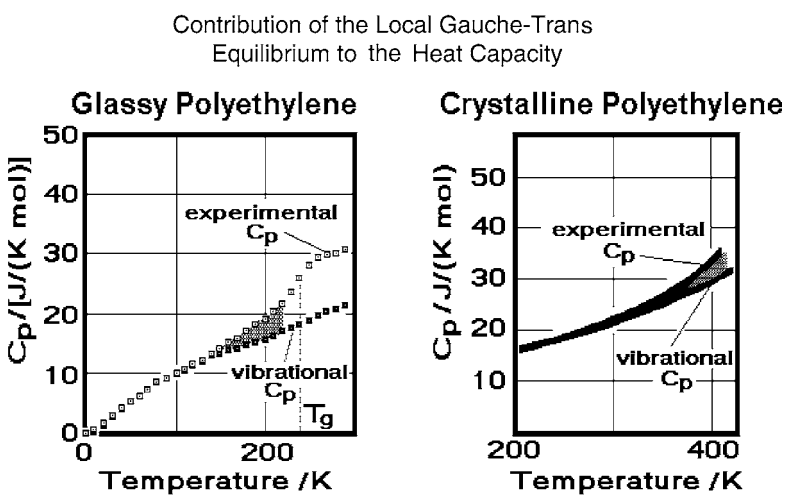

Fig. 3. Contributions of local gauche–*trans* equilibria to the heat capacities of glassy and crystalline polyethylene (shaded area). The vibrational contribution is calculated as described for Fig. 1.

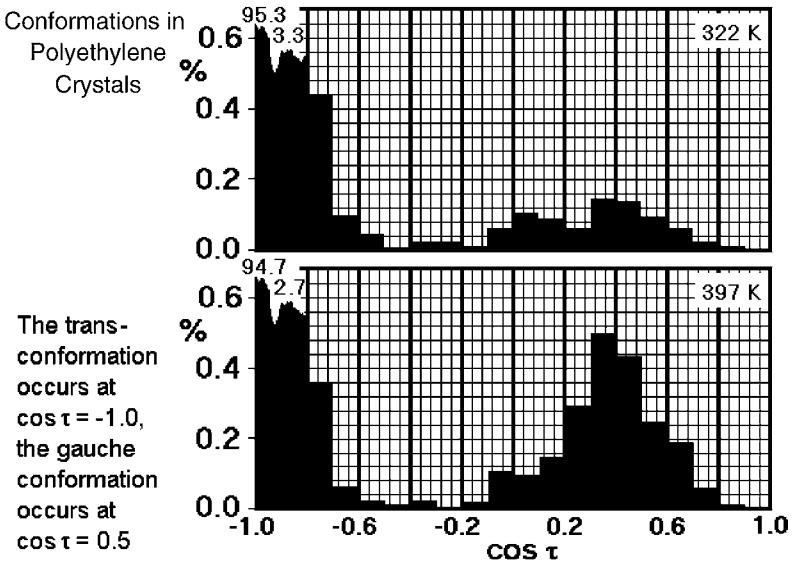

Fig. 4. Distribution of torsional angles τ as obtained by molecular dynamics simulation of 19 polyethylene chains of 100 C-atoms arranged in the orthorhombic crystal structure.

crystals [26]. Two neighboring gauche defects separated by a *trans*-conformation represent a "kink" with a somewhat lower energy within the crystal than two separate gauche defects because of a somewhat smaller distortion of the crystal. The mechanism of kink-formation can be seen in the molecular dynamics simulations of a polyethylene crystal by extracting the conformation of a specific chain at different times.

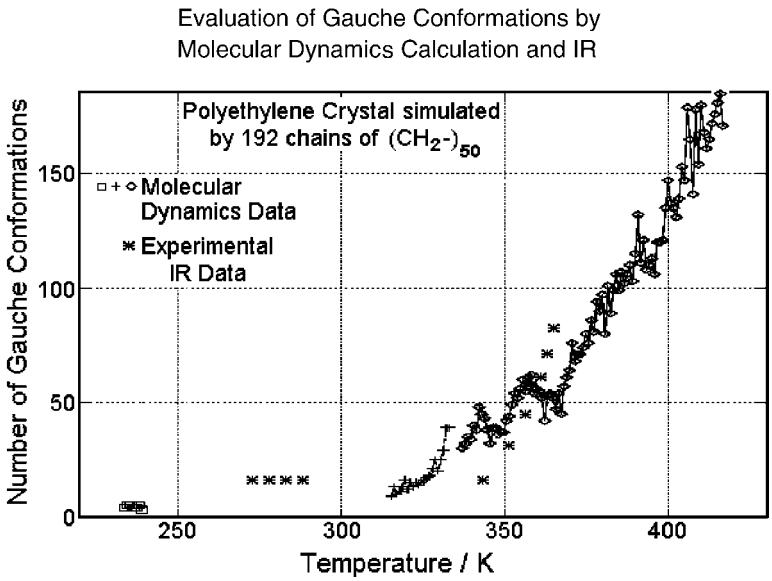

Fig. 5. Concentration of gauche-conformations in crystalline chains of polyethylene from three molecular dynamics simulations over different temperature ranges, compared to experimental data on pentacontae ($C_{50}H_{102}$).

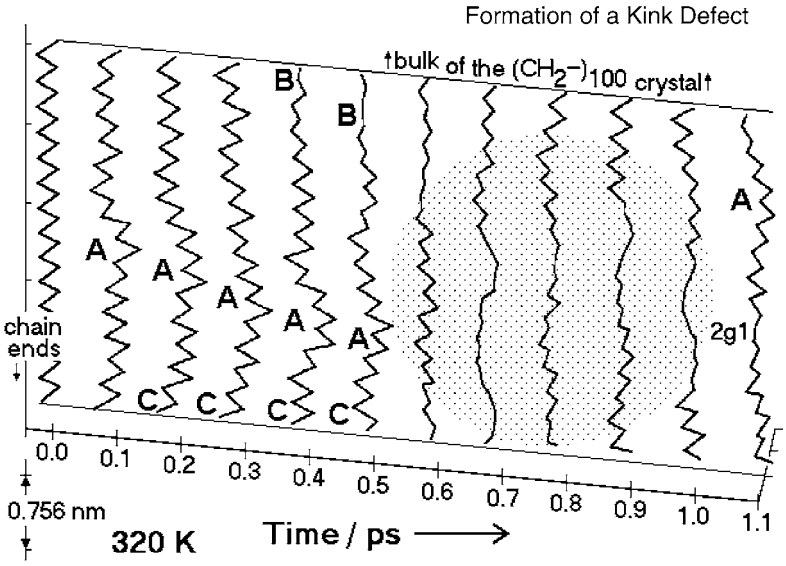

Fig. 6. Details of a 2g1 kink formation by collision of a transverse (A), a torsional (B) and a longitudinal (C) phonon as a function of time (molecular dynamics simulation).

Fig. 6 shows the result. The formation of a transverse skeletal vibration shortly after the beginning of the simulation occurs at position (A) and moves with the speed of sound towards the end of the crystal. At somewhat later time, a torsional vibration appears at (B) in the frame of view and a longitudinal vibration can be seen at (C). Between 0.6 and 1.0 ps into the simulation, all three phonons collide in the shaded area and form the 2g1 kink. The defect keeps a parallel chain arrangement with a twist of 180°, seen best at the bottom of the crystal, and a shortening of the chain by half a unit-cell length. The observed kink had a lifetime of about 2 ps.

The paired gauche bonds within a kink are easier to form than two isolated gauche bonds. Such cooperative motion can be described using the three-dimensional Ising model, as summarized in Fig. 7 [38]. In the lower right of the figure, the energy levels for two defects (DD), one defect (D0), and no defects (00) are indicated and the corresponding energetic parameters are listed. The heat capacity contribution due to the increase in configurations of higher energy is then calculated based on a series of different degrees of cooperativity (Δw). For $\Delta w = 0$, i.e. without cooperativity, one finds a very broad maximum in the heat capacity as is also be derived for a hindered rotator [39]. With increasing Δw, the heat capacity decreases at low temperature because of the increased energy of (D0) and develops an increasingly sharper peak at about 340 K, which ultimately looks like a first-order transition at a critical Δw [40].

In the liquid state, the motion in polymers is characterized by vibrations and conformational changes in an overall amorphous structure. An effort to describe this behavior in calorimetric terms is depicted in Fig. 8 on the example of poly(methyl methacrylate), a polymer with substantial side chains [41]. The heat capacity of the liquid is represented by three contributions, as written in the equation within the heading of Fig. 8. The term C_v (vib) represents the vibrational contribution, calculated as shown in Fig. 1. The ''external'' part (C_{ext}) represents the potential energy introduced by the expansion of the disordered structure. It is approximated by $C_p - C_v$. The third contribution is the conformational contribution which is described in its cooperativity within the repeating unit by a one-dimensional Ising model with a single, low energy ground state for each repeating unit (CH_2–CCH_3(CO–O–CH_3)–) and a single excited state with a degeneracy of Γ. The experimental data, C_p (exp)-liquid, are then fitted in three ways. In the fit (a), all three parameters of the Ising model are taken as

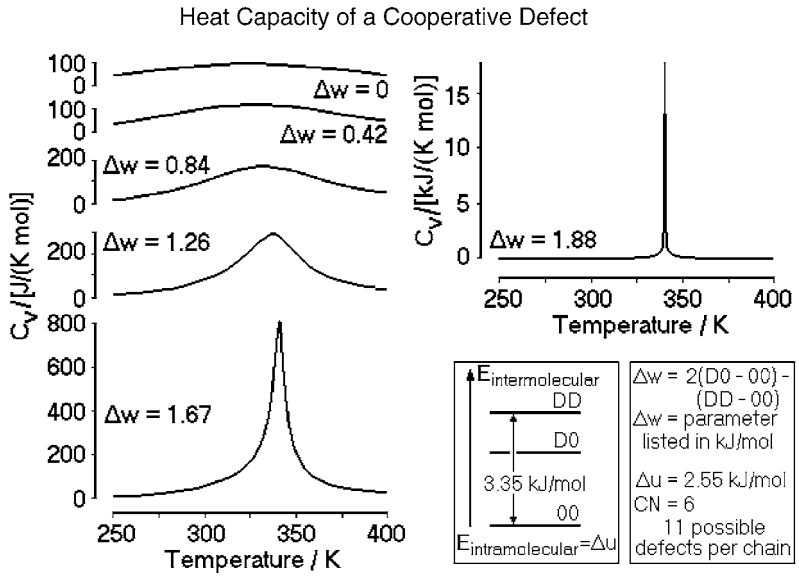

Fig. 7. Computation of the change in contribution to the heat capacity of polyethylene as a function of the cooperativity of the defect formation using the Ising model.

variables (A, the cooperative contribution to B, which is the energy difference between the ground and excited state, and the degeneracy Γ). The calculated data (●) reproduce the experiment well. In the calculation (b) Γ is fixed to the value four, as is sometimes proposed in the literature, but the fit is less perfect (○). Earlier assumptions of A, B, and Γ as given in (c) lead to a fully unsatisfactory fit to the experiment (···). It is of particular interest for the thermodynamic description that extrapolation of these

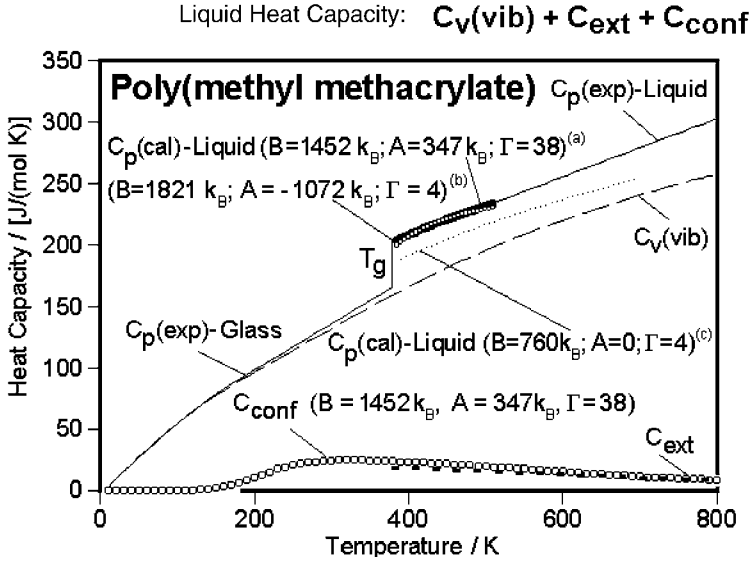

Fig. 8. Heat capacity of liquid poly(methyl methacrylate) and its contributions from the molecular motion.

liquid heat capacities with a fit to the C_{ext} as proposed for the temperature-dependence of $C_p - C_v$ of the crystal by Nernst and Lindemann [34,35] leads for polyethylene to a positive residual entropy at absolute zero, as one would expect from a disordered state. The (unreasonable) straight-line extrapolation of the liquid heat capacity beyond the glass transition temperature, T_g, in contrast, leads to a negative entropy at absolute zero, which is known as the "Kauzmann Paradox" [42]. For the analysis of the entropy of poly(methyl methacrylate), one still obtains negative values, but much less than when using the straight-line extrapolation. These not fully resolved observations present a challenge to derive a self-consistent set of thermodynamic parameters for all polymers and detect possible errors in experimental data such as expansivity, compressibility, and heat of fusion.

As long as the gauche–*trans* interchanges occur in local equilibria, their time scale is still not far from the picosecond scale discussed for the torsional vibrations, and calorimetry can find the appropriate frequencies only by matching C_p to quantum mechanical models. As soon as the large-amplitude motion, however, becomes sufficiently cooperative, slow processes can be studied directly by calorimetry, observing the energetics of an approach to equilibrium. New developments in the various types of temperature-modulated calorimetry (TMC) have recently extended the time scale for calorimetry considerably. This progress was extensively discussed at the sixth Lähnwitz seminar and is contained in this issue of *Thermochimica Acta*. The long-time limit of such experiment is set by the patience of the operator and the sensitivity of the calorimeter, presently set in the megasecond range (10^6 s = 11.6 days). The short-time limit for ac calorimeters approaches at present 2×10^{-5} s or 0.02 ms, 1/200th of the perhaps shortest interval that is humanly discernable. Comparing 1.0 μs as the shortest macroscopic time to the picosecond, characterizing molecular vibrations and torsional jumps, one needs a factor of 10^9. This factor is 100,000 times larger than the factor of 10^4 that separates the microscopic length scale, the ångstrom (0.1 nm), from the macroscopically recognizable lengths in the micrometer range. Perhaps this difference of 5 orders of magnitude in distance from the human level of experience between heat-based molecular motion and mass-based structure is the reason for the slower development of the understanding of calorimetry [28] when compared to molecular structure [43]. For a full description of a material, however, both basic elements, structure and motion must be known. The combination of time and temperature dependence of heat capacity is a topic which may well be central to calorimetry in the 21st century [44].

4. Instrumentation for temperature-modulated calorimetry

The key problem in TMC is to determine the heat flow of a molecular process as it evolves or is absorbed from the sample, and separate it from the effects of heat conduction to the measuring site, usually equipped with a thermocouple or an electrical resistance thermometer. Of the three major types of TMC, the differential scanning TMC method (DSTMC), ac calorimetry, and the 3ω method of measurement, only the first is treated in this paper. The latter two, which reach higher frequencies, are still difficult to calibrate to yield absolute values of heat capacity. The considerable progress in these methods is discussed elsewhere in this issue of *Thermochimica Acta*.

The standard, not-modulated DSC method is easily described as long as one assumes a negligible temperature gradient within the sample and steady state during the period of measurement. Under such idealized conditions, the heat-flow rates of the sample calorimeter (consisting of pan and sample) and the reference calorimeter (usually only an empty pan) are governed solely by the rate of temperature change, $\langle \dot{T}_s \rangle$ (in K min^{-1}), and the heat capacity, $C_s = mc_p + C_r$, where C_s is the heat capacity of the sample calorimeter, m the sample mass, c_p the specific heat capacity of the sample, and C_r the heat capacity of the empty reference calorimeter. The empty sample calorimeter is assumed to have the same heat capacity C_r. In case this is not so, or there exists some other asymmetry in the calorimeters, corrections must be made. Fig. 9a illustrates such a standard DSC experiment, starting at time zero with a linear increase of the temperature of the heater, T_b. After about 100 s, the reference and sample temperatures reach a steady state, i.e. both change with the same $\dot{T}$ as T_b, and ΔT becomes constant. The data in Fig. 9a were calculated by assuming Newton's law constant, K, of

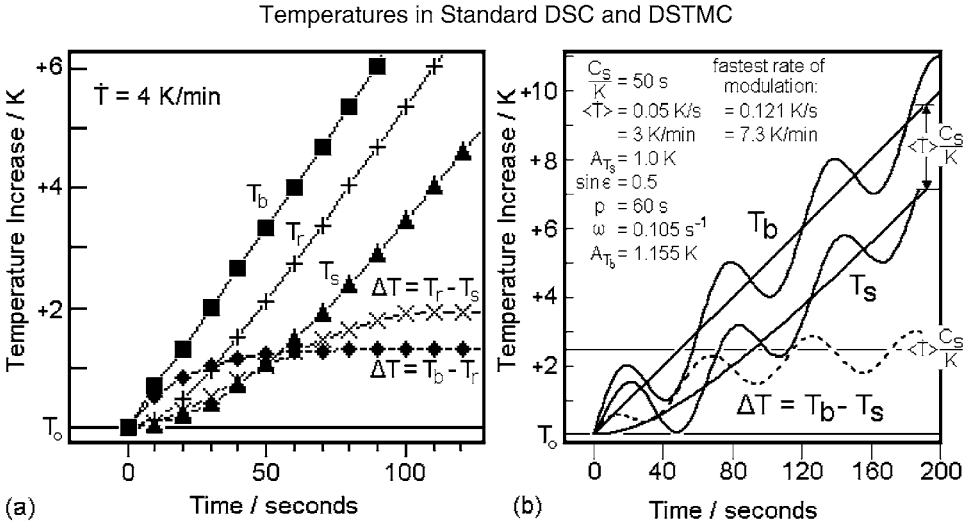

Fig. 9. Temperature changes with time in a standard DSC (a) and a DSTMC (b).

C_r/20 J K^{-1} s^{-1}, and that the Fourier equation of heat flow is valid (see footnote 1). At steady state, the heat capacity is

$$mc_p = K\frac{\Delta T}{\dot{T}} + C_s\left(\frac{d\,\Delta T}{dT_s}\right) \quad (1)$$

where the second term on the right-hand side is a small correction term. The correction is needed since the sample and reference calorimeters change their heat capacities differently with temperature, i.e. T_r and T_s in Fig. 9a are not strictly parallel to T_b. This correction can be calculated and needs no further measurement. The correction is typically of the order of magnitude of 1% as long as mc_p is a substantial portion of C_s. Similarly, to have a negligible temperature gradient within the sample is not a stringent condition as long as steady state is kept. A temperature gradient of 2.0 K across a sample of crystalline polyethylene, for example, will cause an error in the measurement of the magnitude of dC_p/dT, or about 0.3% at 300 K. A survey of many publications used in the ATHAS data bank suggests a standard DSC accuracy of ±3%.

With DSTMC, the measurement of C_p is just as easy, as long as the condition of steady state and negligible temperature gradients within the sample can be maintained, as, for example, with sinusoidal modulation of not too high frequency [4]. In Fig. 9b, the curves illustrate sinusoidal modulation. For simplicity, the heater temperature is modulated. An immediate observation is that the sinusoidal modulation reaches a constant average level after a few cycles, and that the sliding averages over one modulation period $\langle T_b\rangle$, $\langle T_s\rangle$, and $\langle \Delta T_s\rangle$ yield the same curves as seen in Fig. 9a for the standard DSC. Next, a simple subtraction of these averages from their instantaneous values yields the pseudo-isothermal "reversing" signals (the term "reversible" is reserved for proven thermodynamically reversible quantities). Analysis of the reversing heat capacity is possible as long as $\langle T_b\rangle$, $\langle T_s\rangle$, and $\langle T_r\rangle$ change linearly with time. At every time or temperature, $\langle T_s(t)\rangle - T(t)$ is identical to that expected from a quasi-isothermal experiment in which $\langle \dot{T}_s\rangle = 0$. The quasi-isothermal analysis has been described in detail and yields for the heat capacity the following expression which also holds for the pseudo-isothermal case with an underlying heating rate [4,5]

$$C_s - C_r = \frac{A_\Phi K}{A_{T_s}\omega}\sqrt{1 + \left(\frac{C_r\omega}{K}\right)^2} \quad (2)$$

where A_Φ is the modulation amplitude of the heat-flow rate Φ ($\propto \Delta T$) and A_{T_s}, that of T_s. The frequency ω is given in rad s^{-1}. The similarity of Eqs. (1) and (2) becomes obvious if one uses an empty reference

calorimeter for the measurement. Then, $C_s - C_r = mc_p$, and $A_{T_s}\omega$ represents the amplitude of the modulation of the rate of temperature change without the effect of the underlying rate, $\dot{T}(t) - \langle\dot{T}\rangle$. The square root accounts for the difference between the modulation of reference and sample calorimeters. Note, however, that if calibration and measurement are done at the same frequency and the reference pans do not change between runs, the square root part of Eq. (2) is constant and can be included in the calibration constant.

The just discussed Eqs. (1) and (2) hold only if steady state is not lost during modulation and the temperature gradient within the calorimeters is negligible. This condition is more stringent for DSTMC than for the standard DSC, because if even a small temperature gradient is set-up within the sample during the modulation, each modulation cycle has smaller positive and negative heat flows which depend on the unknown thermal conductivities. A negligible temperature gradient within the sample requires, thus that the sample calorimeter oscillates in its entirety. It also requires a negligible thermal resistance between thermometer and pan, and the pan and sample calorimeter. The phase lag ε between heater and sample must be entirely due to the thermal diffusivity of the path to the sample ($T_s(t) = A_{T_s}\sin(\omega t - \varepsilon)$). Typical conditions that need to be applied for measuring C_p of polymers with sinusoidal modulation are masses of 10 mg or less, amplitudes of 1.0 K or less, and modulation periods of 60 s or longer. These are smaller masses and heating rates than possible for the standard DSC and diminish the advantages gained by DSTMC due to its rejection of spurious heat losses that do not match the frequency of analysis, namely ω.

An analysis of the temperature distribution within a power-compensated DSTMC was done using infrared thermography as is illustrated in Fig. 10 [45]. The observed temperature distribution within an open sample cell is shown in Fig. 11. Clearly, the modulation amplitude decreases and a phase shift develops between bottom and top of the sample. It is impossible to handle such data with Eq. (2). Progress was made by studying DSTMC with sawtooth modulation. In this case, the input parameters for the experiment can be the same as used for the standard DSC in Fig. 9a, just that the heating rate is changed periodically to cooling and back to heating. As long as the Fourier equation of heat flow holds, the solutions for different events in the DSC are additive. Steady state, however, is lost each time a sharp change of $\dot{T}_s$ occurs. Attempts were made to use the maxima and minima of the modulation response. This, however, corresponds to a standard

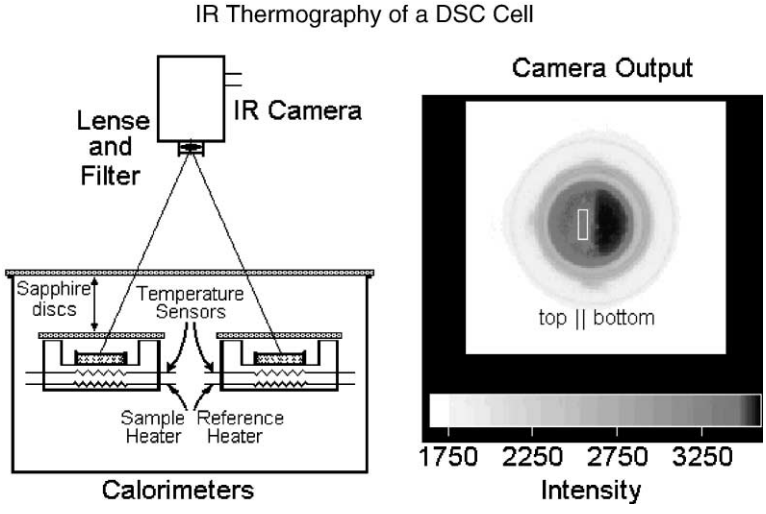

Fig. 10. Experimental set-up and data recording for contact-less infrared thermography. Access to the bottom of the open sample pan on the right, and the top of the half sample on the left is enabled by the IR-transparent sapphire discs. The rectangle marks the size of the area averaged for measurement.

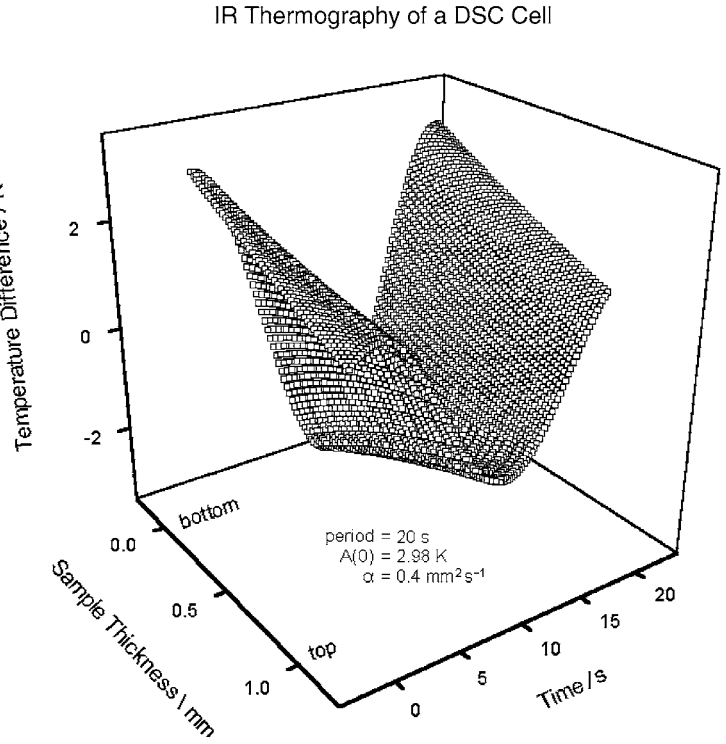

Fig. 11. Result of infrared thermography during DSTMC calculated using the experimentally determined amplitude reductions from the programmed amplitude of 4–2.98 K at the bottom of an uncovered 1 mm thick poly(ethylene-co-octene) sample and 1.47 K at the top.

DSC test for the reversing nature of the sample and loses the advantages of DSTMC. Furthermore, it is only correct if steady state is reached at the end of each half cycle. Investigations of the sawtooth modulation brought a number of interesting results. It could be shown that if there were no temperature gradients within the sample and if all other lags and gradients could be assessed with the Fourier heat-flow equation, Eq. (2) does allow the calculation of the precise heat capacities [10]. An analysis without temperature gradient within the sample is, however, rarely possible because of the small sample mass required. An empirical solution was to modify Eq. (2) such that [46]

$$C_s - C_r = \frac{A_\Phi K}{A_{T_s}\omega}\sqrt{1+(\tau\omega)^2} \tag{3}$$

where τ is a characteristic time constant for the measuring system and has the dimension s rad^{-1}. It can be determined by measurements at different frequencies. The characteristic time, τ, does not only depend on the heat capacity of the reference calorimeter and the Newton's law constant, as one would expect from Eq. (2), but also on the mass and thermal conductivity of the sample, and on all involved thermal contacts. Furthermore, the nature of τ depends also on the calorimeter type, and naturally also on any possible cross-flow between the sample and reference calorimeters.

Modeling of such complicated situations has been attempted for a heat-flux calorimeter by using an analog electrical circuit as is illustrated in Fig. 12 and results in [47]

$$C_s - C_r = \left(\frac{2R+R'}{RR'}\right)\frac{A_\Phi}{A_{T_s}\omega}\frac{\sqrt{1+(\omega C_s R_s)^2}\ \sqrt{1+(\omega C_r)^2(R_r+(RR'/(2R+R'))^2}}{\sqrt{1+(\omega C_s C_r((R_s-R_r)/(C_s-C_r)))^2}}. \tag{4}$$

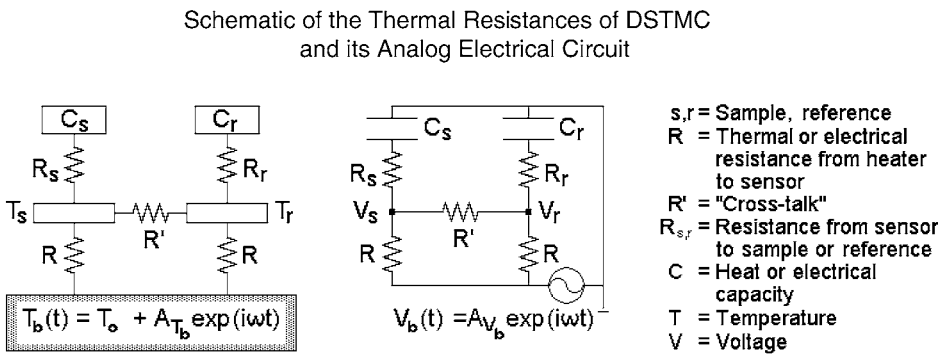

Fig. 12. Thermal resistances in a heat-flux type DSTMC and the electric circuit equivalent which leads to Eq. (4).

The modulated temperature is generated at the heater, $T_b(t)$, and causes heat flows to the sample and reference temperature sensors, T_s and T_r, both retarded by the identical thermal resistances R and with a possible cross-flow, hindered by R'. The final step is the conduction of the heat from the temperature sensors into the calorimeters, hindered by the resistances R_s and R_r. Note that the temperature gradient shown in Fig. 11 is not considered. It would complicate Eq. (4) even further.

Eq. (4) can be seen to link to Eq. (2) by simply setting $R = 1/K$, $R_s = R_r = 0$, and $R' = \infty$. It was impossible, however, to apply Eq. (4) to the experimental data [47]. As a result, we decided to use the empirical Eq. (3) for the data analysis. As long as only sample mass and thermal conductivity are affecting τ (in addition to C_r and K), a plot of the inverse of the uncorrected heat capacity of Eq. (3) versus the square of the frequency should be linear, and τ, independent of ω. Only with periods beyond about 250 s does the square root term become negligible in Eq. (3) when analyzing heat capacities typical with commercial calorimeters.

For the computation of the amplitude of the heat-flow rate, A_Φ, and analogously the amplitude of the sample temperature, A_{T_s}, one uses the Fourier series

$$\Phi(t) = \langle\Phi\rangle + \sum_{n=1}^{\infty}[A_n \sin(n\omega t) + B_n \cos(n\omega t)] \qquad (5)$$

where A_n and B_n are amplitudes that must be determined in the usual manner, and n, an integer and represents the order of the harmonic. As long as the modulation is symmetric about $\langle\dot{T}\rangle t$, and begins at time $t = 0$, it is centrosymmetric and all B_n are 0, i.e. the series contains only the sinusoidal harmonics. For a linear response of the sample to a sinusoidal modulation, no higher harmonics are generated in the heat-flow rate, i.e. in Eq. (2) $A_\Phi = A_1$. A centrosymmetric sawtooth modulation also simplifies the Fourier representation, it shows only odd, sinusoidal harmonics with $n = 1, 3, 5, 9$, etc.

$$\Phi(t) = \langle\Phi\rangle + \frac{8A_\Phi}{\pi^2}\left[\sin\omega t - \frac{1}{9}\sin(3\omega t) + \frac{1}{25}\sin(5\omega t) - \frac{1}{49}\sin(7\omega t) + \frac{1}{81}\sin(9\omega t) - \cdots\right]. \qquad (6)$$

If Eq. (6) describes the modulation and response of a DSTMC, each sinusoidal harmonic can separately be used to compute the heat capacity. Such analysis is illustrated in Fig. 13 for a typical copolymer, analyzed with a Mettler–Toledo calorimeter [48]. Several runs with different modulation periods and their higher harmonics were used, and the uncorrected heat capacities are plotted as calculated from Eq. (3) with K set equal 1.0. The plot on the right illustrates the evaluation of τ, used to extrapolate to frequency zero. Note that the calibration run with sapphire can only be used after evaluation of its separate τ value and extrapolation to zero frequency. It could also be shown that the common practice of subtracting a baseline of a run with two empty calorimeters to correct for the asymmetry is not mathematically sound, but for highest precision must similarly be converted to heat capacity at zero frequency [22].

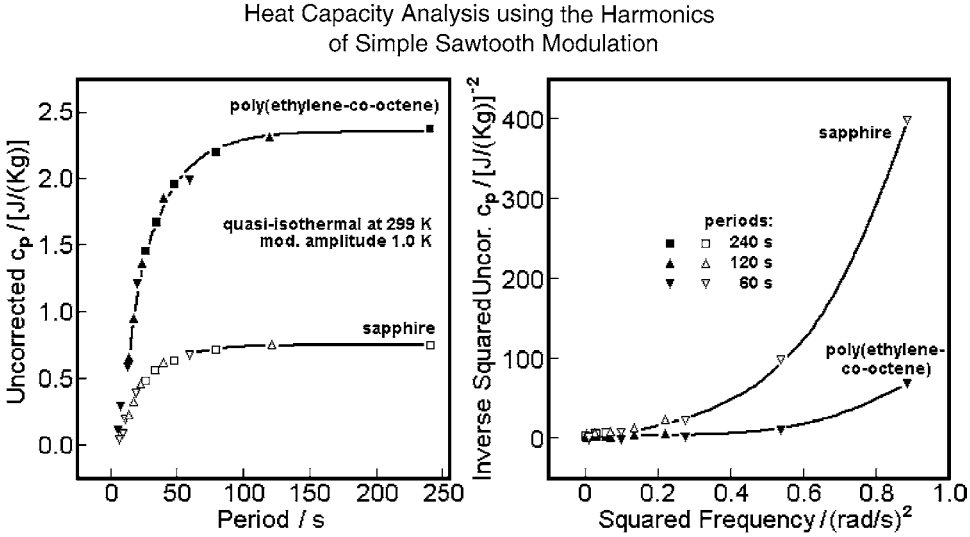

Fig. 13. Heat capacity by quasi-isothermal DSTMC calculated from the harmonics of $n = 1$–9 of simple sawtooth modulations with three different base frequencies (60, 120, and 240 s for $n = 1$). Measurements for a copolymer of polyethylene and sapphire (Mettler–Toledo DSC).

The final step in the analysis is to eliminate the problem that arises for the use of multiple frequencies from the quickly decreasing amplitudes of the higher harmonics in Eq. (6). This is accomplished by replacing a simple sawtooth with one designed to have similar amplitudes for the temperature amplitudes of the first, third, fifth, and seventh harmonics and much smaller ones for the subsequent amplitudes [22]

$$T(t) - T_0 = A[0.378\sin\omega t + 0.251\sin(3\omega t) + 0.217\sin(5\omega t) + 0.348\sin(7\omega t) - 0.067\sin(9\omega t)\cdots] \quad (7)$$

or by using step-isotherm or related modulations

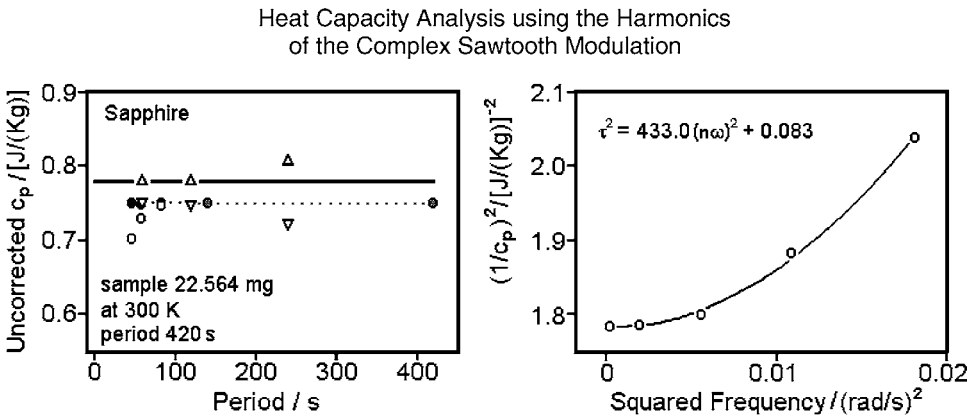

Fig. 14. Heat capacity by quasi-isothermal DSTMC with the harmonics 1–9 of a complex sawtooth as given by Eq. (6). Measurements for sapphire. Open circles (○), calculated for the harmonics 1–9, using Eq. (2) with $K(n\omega) = 1$ (uncorrected). Filled circles (●), corrected according to Eq. (3) with τ determined from the quadratic fitting. Shaded circles are superimposed (○ and ●). The data marked (△) and (▽) are less accurate standard DSC evaluations on heating and cooling, respectively, gained from segments of the sawtooth that had reached steady state (Mettler–Toledo DSC).

which result in similar heating-rate amplitudes for all harmonics in the Fourier series [49].

Heat capacity with a precision approaching 0.1% could be measured with such modulations using the usual sequence of a calibration run with sapphire, an asymmetry calibration with two empty pans, and the sample run. A single measurement gives then enough data at different frequencies to analyze the data, as shown in Fig. 14 for a measurement with the Mettler–Toledo DSC [24]. Similar experiments were also carried out with the standard DSC of T.A. Instruments [23,49], and the power-compensation calorimeter by Perkin-Elmer [25,49]. In all cases, there was a significant improvement of the precision. All runs needed separate evaluation with a different τ. Even changes in sample and pan shapes and positions change the value of τ. In all cases, the thermal resistances in Fig. 13 produce temperature gradients that depend on ω, and can in this way be corrected for. Analyses of this type were performed with all major commercial calorimeters using the higher harmonics of slower modulations. Harmonics with frequencies as high as 0.1 Hz could be used for such analyses.

5. Latent heats as found in glass transitions, crystallization, melting, and crystal perfection

A second quantity measured by calorimetry is the latent heat, L. In contrast to the heat capacity, C_p, described in Sections 2 and 3, its absorption or evolution by the sample causes no change in temperature, but depends on the progress of the process, $x[L = \int(\partial H/\partial x)_T \, \mathrm{d}x]$. To evaluate the change in enthalpy, ΔH, the latent heat must be added to the heat capacity contribution and the change of C_p must be considered as the process progresses which involves the latent heat. For melting at a constant temperature, T_m, for example, one can write $\Delta H = \int_{T_1}^{T_\mathrm{m}} C_p(\mathrm{solid})\,\mathrm{d}t + L + \int_{T_\mathrm{m}}^{T_2} C_p(\mathrm{liquid})\,\mathrm{d}t$, where T_1 and T_2 specify the temperature interval of interest.

In case the evolution or absorption of a latent heat occurs over a wide temperature range and is of similar magnitude to that of the heat-capacity contribution over the same temperature range, both contributions may at first be calculated together from the appropriate heat-flow rates and calculated from Eqs. (1)–(3) as an ''apparent'' heat capacity. The separation of the apparent heat capacity into the true heat capacity and the latent heat is easiest when the latent-heat contribution is fully irreversible and constant with temperature over the amplitude of modulation. When measured by DSTMC over a sufficient number of modulation cycles, the irreversible latent heat effect is then fully separable from the reversing heat capacity. In this case, the reversing signal is due to the heat capacity alone, and the total heat-flow rate contains both the heat capacity and the latent heat contribution. Typical examples are the cold crystallization of polymers, non-equilibrium reactions such as degradation or cross linking, and to some degree also the separation of the enthalpy relaxation during the glass transition.

If the irreversible process has a measurable temperature dependence, Toda has developed a model to extract the rate of change of the irreversible process from the frequency dependence of the reversing signal [50]. For the application of this method, one must be sure that all instrument lags are properly accounted for, and no other processes with latent heats occur at the same time, such as crystal perfection during melting or after crystallization.

Special techniques must be applied for sharp transitions involving latent heats because of difficulties of separating the modulation effect from nonlinear changes in latent heat. Usually, it is best to use a standard DSC and an interpolated baseline to separate the transition peak which is commonly broadened due to the instrument lag. Similarly, slow processes such as crystallization and annealing of crystals must be treated in a special fashion. Typically, isothermal DSC can be applied to measure irreversible latent heats directly or, quasi-isothermal DSTMC can be used to evaluate the change in reversing heat capacity which is linked to the change in composition of the sample. The determination of latent heats in two transitions will be summarized and updated on examples of polymers, namely the glass transition [9,11–14], and the melting transition [10,15–18]. Evaporations, mesophase transitions, and chemical reactions have been treated analogously and have also been discussed in the various Lähnwitz seminars [6–8].

In the glass transition region the conformational changes and the external contribution in the liquid, as described in Figs. 3 and 8, are sufficiently slow so that their kinetics is measurable by DSTMC. An early and

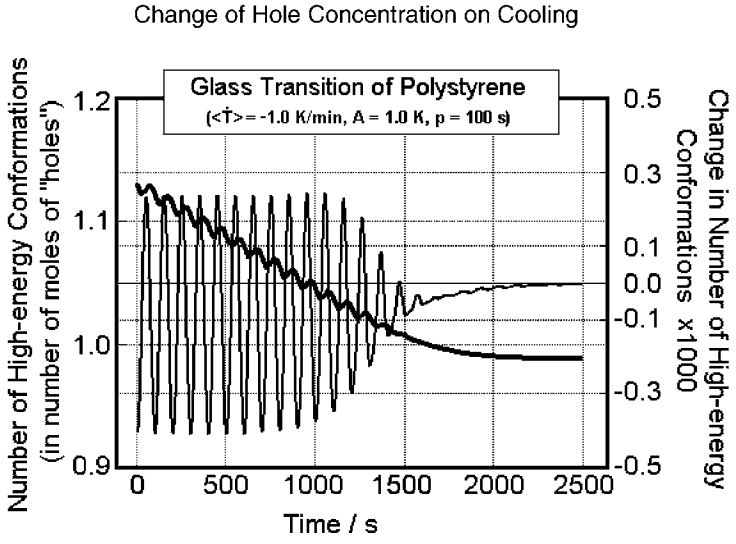

Fig. 15. Calculations on cooling in the glass-transition interval using the hole theory.

simple description of this behavior is given by the hole model of the glass transition developed by Hirai and Eyring [51]. The holes are described by high-energy conformations with a fixed volume related to the geometry of the molecular packing and a hole energy, estimated from the cohesive energy of the material. When the hole theory was first used to interpret results by dynamic differential thermal analysis, DDTA, it was found that the hole model does not fully account for the cooperativity of the glass transition and one could model the process only approximately [52]. Using the glass transition of polystyrene as an example, the changes on hole concentration on cooling and heating were calculated on the basis of new DSTMC data [11], as is illustrated in Figs. 15 and 16 [12,14]. Fig. 15 shows how on cooling the modulation amplitude decreases as one progresses through the glass transition. At the same time, however, there is also a

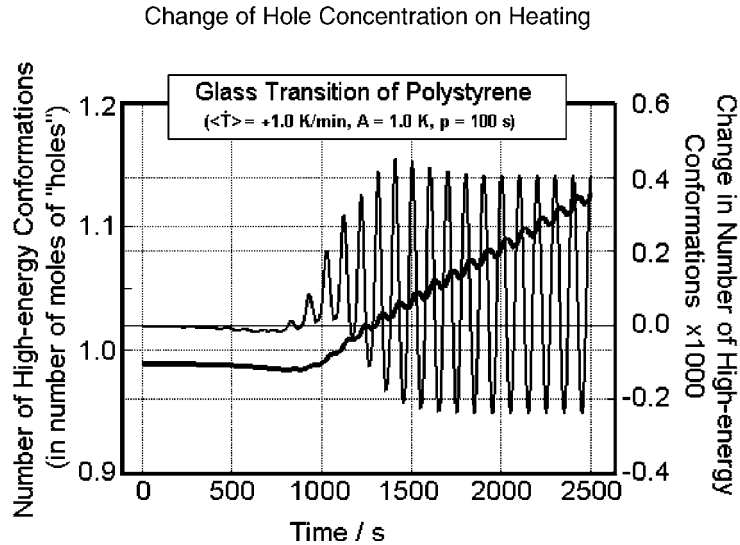

Fig. 16. Calculations on heating in the glass-transition interval using the hole theory.

continuous decrease in hole concentration due to the underlying cooling rate which leads to an easily recognizable asymmetry of the modulation, best seen in the plot of the change in number of high-energy conformations (holes). The plot of the heating of the sample cooled as given in Fig. 15 is given in Fig. 16. As the glass transition is approached, there is first a decrease in concentration of holes which should give rise to an exothermic hysteresis peak, followed by the approach to the average change of hole concentration with temperature in the liquid state. The effect due to the underlying heating rate is not modulated, and appears in the nonreversing heat-flow rate of the experiment which is reproduced in Fig. 17 as an enthalpy relaxation. The enthalpy relaxation is largely irreversible and represents a latent heat which depends on the level of hole concentration which froze on cooling in relation to the heating rate for analysis. A more slowly cooled sample, as well as a sample which was annealed below the glass transition temperature, has a lower hole concentration and exhibits a larger endothermic enthalpy relaxation on faster heating. The exothermic enthalpy relaxation is always present during since the sample anneals while approaching the glass transition, as seen in Fig. 16 and also visible in the experiment of Fig. 17 in the nonreversing maximum before the larger minimum. Analyzing a quickly cooled sample by slow heating should give an analogous exotherm to the endotherm, but is usually much smaller than expected [52]. This discrepancy between model and experiment is likely due to a larger cooperativity at lower temperature which is not describable by a simple temperature-dependent relaxation time.

It interesting to note that in this way the glass transition, which ideally occurs without heat or entropy change at the temperature T_g, may show a latent-heat effect due to the kinetics of the enthalpy relaxation. Furthermore, the dynamic response of the glass transition is certainly reversing as illustrated in Figs. 15 and 16, and seen in Fig. 17. The transition as a whole, however, is thermodynamically irreversible, since the equilibrium state is at all temperatures that of the liquid. It can be reached below the glass transition temperature only when extrapolating the DSTMC results to frequency zero. Below the glass transition temperature this state cannot be reached in the available time for measurement.

The descriptions given in Figs. 15 and 16, however, are only approximate. The behavior of a sample in the glass transition region is typically nonlinear [53]. There exist problems in the response of the sample to the modulation by generating higher harmonics due to the change of the relaxation-time with temperature

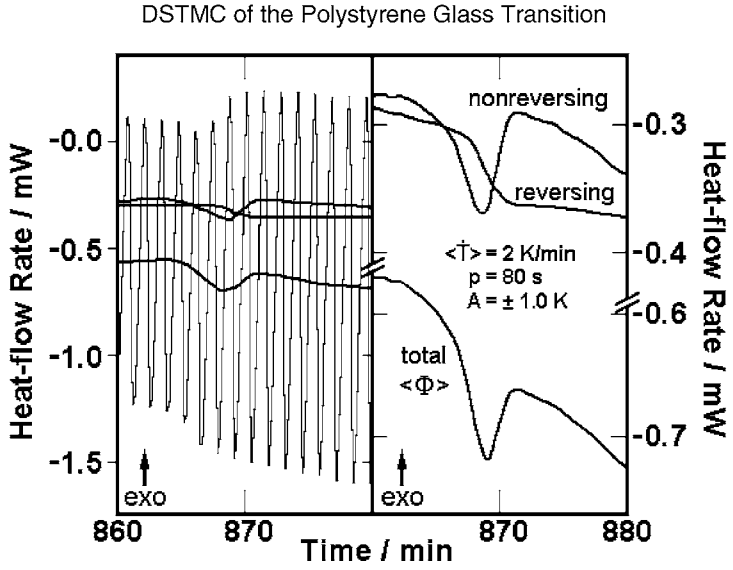

Fig. 17. Example of DSTMC of polystyrene with a T.A. Instruments calorimeter with sinusoidal modulation. The right curves are expanded.

[12]. In addition, frequency shifts are introduced in the glass transition region due to an interference between the time scale of the underlying heating rate and the modulation [14]. Finally, there is a measurable decrease in the relaxation time with the hole concentration itself [11]. The frequency dependence of the glass transition should thus be analyzed at constant hole concentrations, an experiment that may be possible by simultaneous modulation with several frequencies, as described, for example, by Eq. (7) or by measurement at a sufficiently high temperature and frequency so that only the reversing dynamic glass transition is measured. A first example of an analysis with multiple frequencies is shown in Fig. 18. The characteristic times, τ, were taken from analyses as shown in Figs. 13 and 14 [49,54]. Outside the transition region the characteristic time changes only little with temperature, while in the glass transition region a large change is visible that is responsible for the frequency dependence of the apparent reversing heat capacity in the glass transition region, as shown in Fig. 19. Measurements of such type may allow to study the dynamic glass transition due to modulation alone at a constant number of non-equilibrium holes.

The problems with the analysis of reversible melting are reviewed in Fig. 20 on hand of the example of indium [10]. As long as the melting is incomplete so that enough crystal nuclei remain for crystallization on cooling, the melting is reversible over a temperature range of ± 0.05 K or less [55]. The analysis of transition peaks with DSTMC which are narrower than the change of the underlying temperature of one modulation period involves more than one melting and crystallization process of the same crystals so that the reversing signal is larger than expected for a single transition (see Fig. 20). Furthermore, both the total heat-flow rate $\langle \Phi(t) \rangle$ and the reversing heat-flow rate amplitude A_Φ are broadened beyond the actual widths of the transitions due to the fitting procedure to a Fourier series. Finally, higher harmonics which are generated by the sharp transition peaks, are not considered in the computation of A_Φ. This makes the standard DSC more suitable for the analysis of sharp melting materials. It needs only corrections for the instrument lag. If superheating or supercooling is possible, the kinetics can be assessed with isothermal calorimetry or quasi-isothermal DSTMC, as mentioned at the beginning of this Section.

Linear high polymers were considered not to melt or crystallize reversibly [19]. In this case, the reversing heat capacity should not show any latent heat contribution as is usually the case for cold crystallization [1–3,15]. In most experiments carried out since the

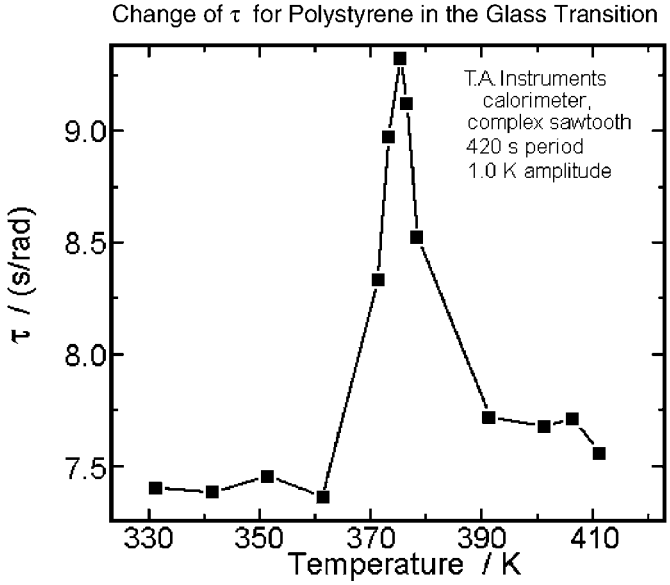

Fig. 18. Time τ in the glass transition region, as determined from Eq. (3).

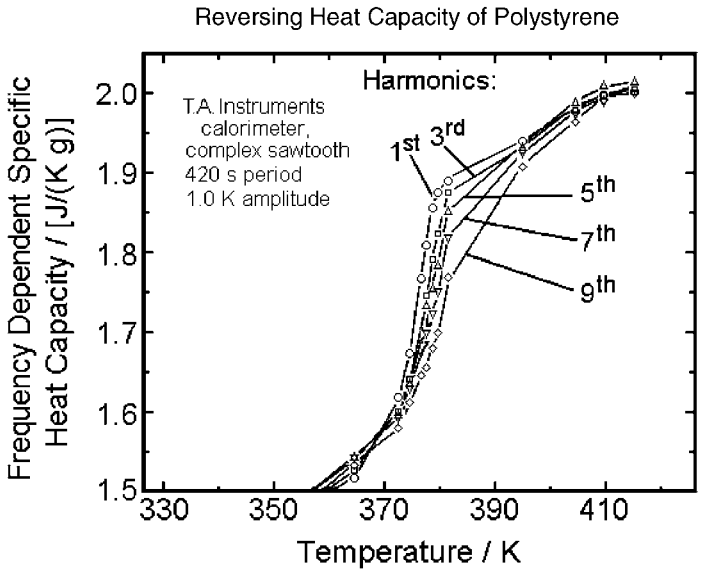

Fig. 19. Apparent, reversing heat capacity in the glass transition region as a function of frequency. Sawtooth modulation as given by Eq. (7).

first quantitative analysis [9,16], however, some reversing component was observed. The reversing latent heat can be separated into at least two effects, as is illustrated in Fig. 21 on the example of quasi-isothermal analysis of poly(oxyethylene) (PEO) of low molar mass (≈1500 Da) [17,18]. A poorly-crystallized sample shows a very small reversing melting peak. Subsequent cooling using the step-wise quasi-isothermal analysis shows no peak of reversing melting and only very little supercooling. Subsequent reheating shows also practically no reversing melting peak. A more detailed analysis of the small reversing peak is possible when analyzing the Lissajous figures at different modulation amplitudes, as shown in Fig. 22.

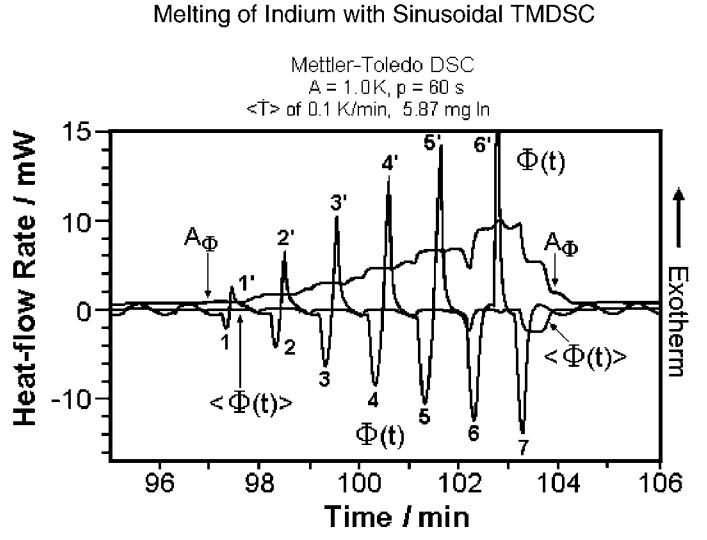

Fig. 20. Melting of indium as analyzed using Eq. (2).

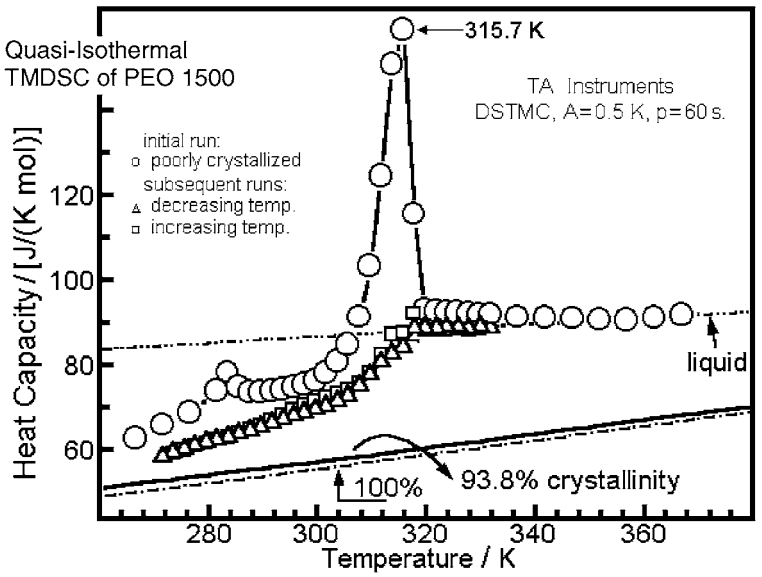

Fig. 21. Reversing heat capacity of poly(oxyethylene) in the melting region. Data points evaluated between 10 and 20 min of quasi-isothermal, sinusoidal modulation.

Small-amplitude modulation shows no melting or crystallization, larger amplitudes develop melting and crystallization, but at different temperatures. The supercooling necessary for crystallization seems to be constant with temperature and the crystallization kinetics determines the amount of crystallization. Melting, in turn, begins at different temperatures for the different modulation amplitudes, suggesting poorer crystallization for the larger modulation amplitudes (at constant frequency). The second effect is a higher apparent C_p than expected for the 98.3% crystalline samples. This truly reversible melting is

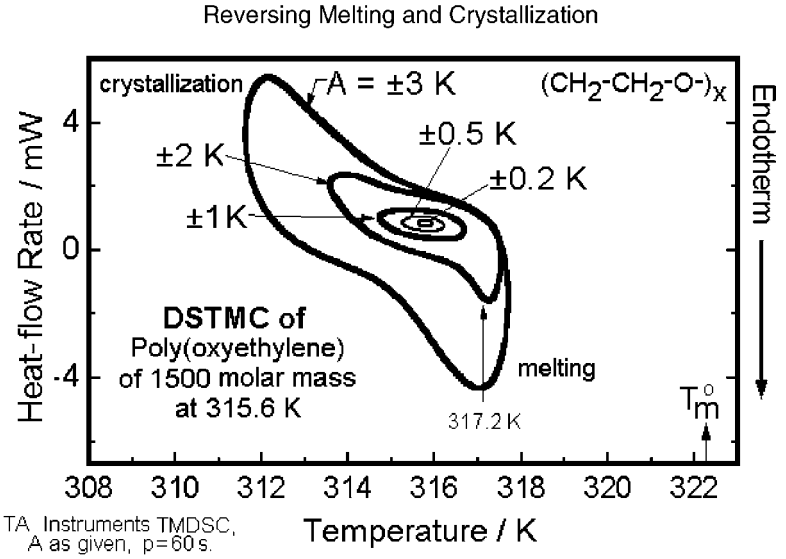

Fig. 22. Lissajous figures at 315.6 K for the experiment of Fig. 21 at different modulation amplitudes (sinusoidal modulation).

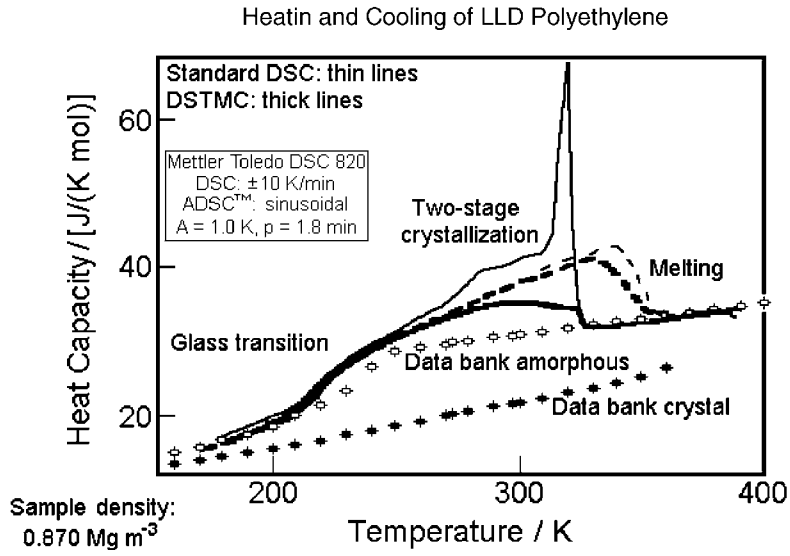

Fig. 23. Heat capacity of PEcoO as determined by various calorimetric techniques on cooling and heating through the melting region. Continuous lines indicate analysis on cooling, broken lines on heating.

the subject of the following discussion and has been observed for most of the polymers analyzed to date [15–18,56]. The next paragraphs summarize recent progress.

Poly(ethylene-co-octene-1)s crystallize as polyethylene crystals and are also called linear low-density polyethylenes (LLDPE) as long as the octene-1 concentration is small. Fig. 23 summarizes their thermal analysis on heating (dashed lines) and cooling (solid lines) with standard DSC (thin lines) and DSTMC (heavy lines) [20,21]. In addition, the vibrational heat capacity (closed symbols) and the liquid heat capacity and the glass transition (open symbols) are marked as they are known from the ATHAS Data Bank [29]. The first stage of crystallization is largely irreversible, but much of the second stage appears in the reversible part of the DSTMC and continues to contribute a latent heat until the temperature reaches the glass transition at about 210–250 K. To understand the details of this surprising crystallization and melting experiment, long-time quasi-isothermal DSC and DSTMC experiments were carried out at various temperatures. Fig. 24 illustrates the change in the reversing apparent heat capacity that occurs at 299 K when interrupting the cooling displayed in Fig. 23. Extrapolating the heat capacity to very long times results in a fully reversible latent heat capacity at 299 K that is larger than expected from the data bank data for crystalline and melted polyethylene in the proper proportion, i.e. it must contain a latent heat contribution. Two relaxation times are needed for the fit of the data of Fig. 24 and are interpreted as being due to secondary crystallization and crystal annealing. Annealing of the sample at the same temperature for various times to extend the kinetic data to 0.3×10^6 s was followed by continued cooling and reheating under standard DSC conditions and led to the results shown in Fig. 25. The annealing reduced the number of crystals that were melting before the annealing in the 299 K region, and increased the crystals melting at higher temperature, as expected for an annealing peak [19]. Before any annealing occurred, an additional endotherm developed, as marked in Fig. 25 by the arrow (↘), and is taken as an indication of some secondary crystallization. Analyzing the DSTMC data in the time domain supports the DSC result, as illustrated in Fig. 26. The reversible heat-flow rate shows an initially larger exotherm before it approaches a reversible shape with almost equal exotherms and endotherms added to the heat capacity required from vibrations and large-amplitude motion, as described in Sections 2 and 3.

The interpretation of Figs. 23–26 led to the following six contributions to the thermal analysis with time scales ranging from picoseconds to megaseconds. The

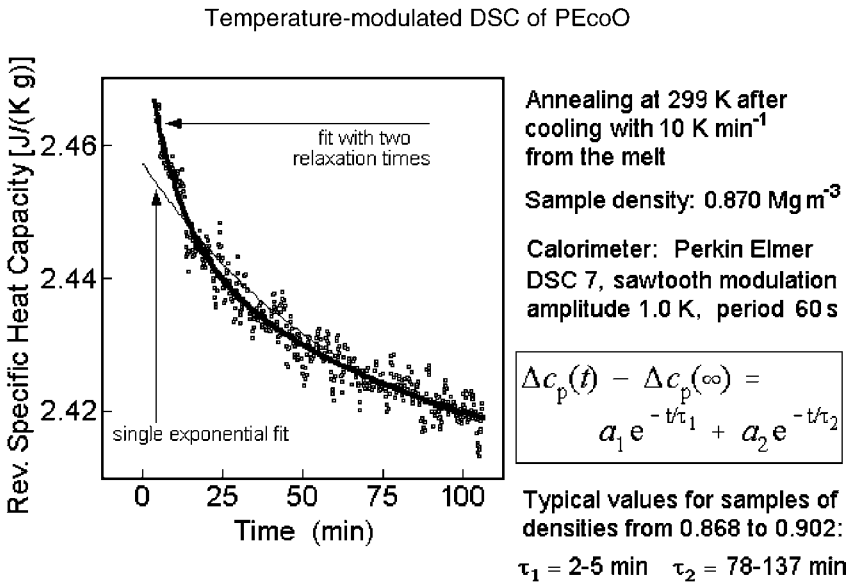

Fig. 24. Change of the apparent reversing heat capacity of PEcoO with annealing time at 299 K after cooling the sample to this temperature as in Fig. 24.

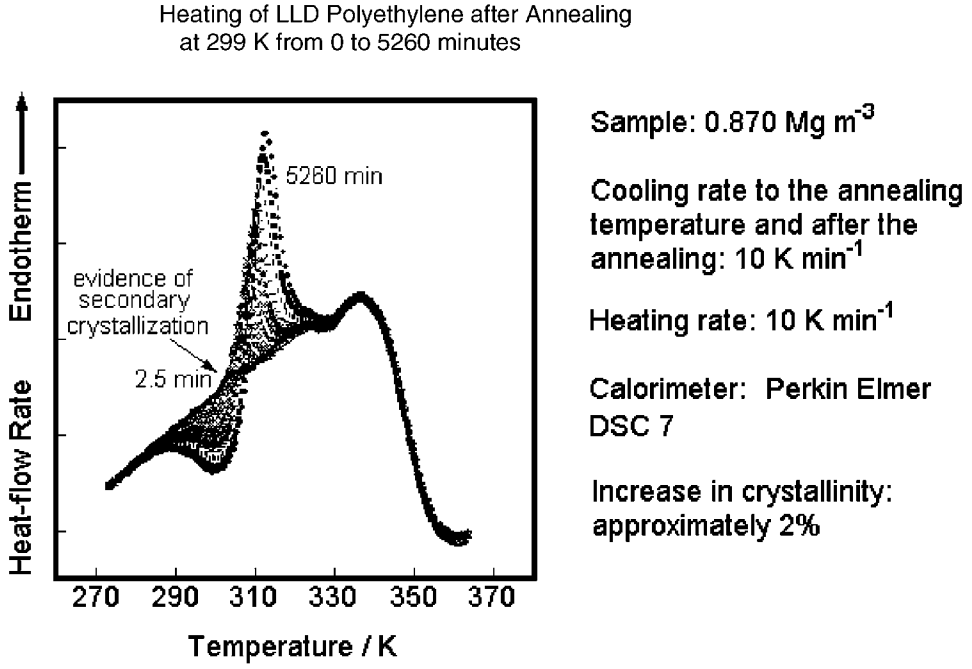

Fig. 25. Standard DSC heating traces of PEcoO after annealing as indicated in the figure (compare to the standard DSC heating trace without annealing in Fig. 24).

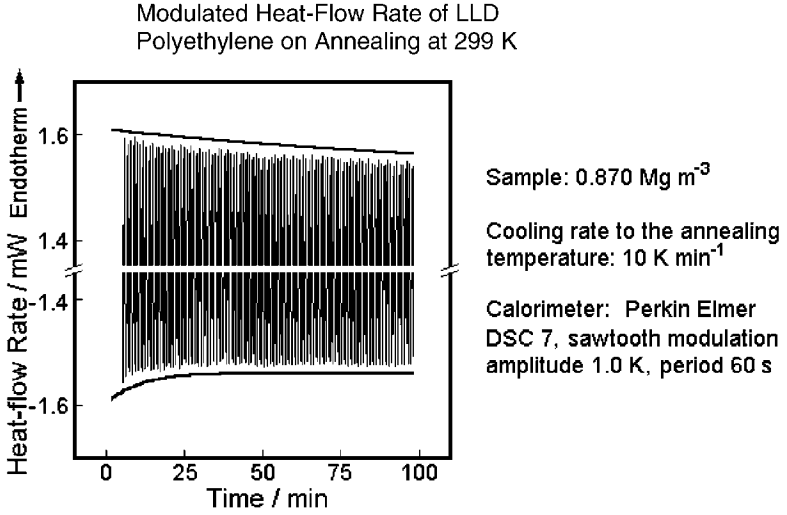

Fig. 26. Heat-flow rate data of the annealing of PEcoO shown in Fig. 25.

first three are truly reversible: the vibrational heat capacity (1) as described in Section 2, the gauche–*trans* equilibrium (2) as discussed in Section 3, and the reversibly melting fraction (3) as found after long-time annealing at temperatures lower than ultimate melting. The second three contributions are increasingly more irreversible. They consist of crystal perfection, with a 100 min relaxation time for PEcoO at 299 K (4), and secondary crystallization with a time constant for PEcoO of approximately 5 min at 299 K (5). Both, contributions (4) and (5) may contribute to the annealing peak with a temperature difference between formation and melting of 5–15 K. Finally, primary crystallization and melting (6) is commonly the biggest effect and shows temperature differences between crystal growth and melting of usually 10–30 K. It can be seen as the sharp initial crystallization peak in Fig. 23.

The reversible melting just described is a phenomenon which cannot be explained with classical theories of melting and crystallization of polymers, where the phase transformation from the solid crystalline phase to the melt and vice versa is considered to be an irreversible process. Crystallization should always occur via nucleation with supercooling (i.e. the creation of the appropriate nuclei), followed by crystal growth, and perfection [19]. After crystal growth and perfection are completed, melting can only occur at a considerably higher temperature. Although crystal nucleation can be avoided by seeding with heterogeneous nuclei or incomplete melting, molecular nucleation cannot be avoided. It allows the addition of a new molecule to a growing crystal. The heating and cooling cycles in the PEcoO are, however, fully reversible and independent of modulation amplitude, i.e. molecular nucleation had been eliminated. The explanation for such reversible crystallization and melting must be that small chain segments arrested on one or both sides on the surface of higher melting crystals are involved in the process. It is known, for example, that side-chains of polymers, as soon as they are tied to the main chain with a flexible spacer of four to eight CH_2-groups can crystallize and melt similar to the corresponding small molecule, i.e. crystallize and melt reversibly with melting temperatures not far from the small molecules, severed from the main chain [19]. The analysis temperature of 299 K which is used in Figs. 24–26, for example, could correspond to the melting temperature of segments of 20–30 CH_2-groups. Paraffins of this length show no supercooling [10]. Two locations offer themselves in the structure of semicrystalline polymers for such chain segments. One is found for chain segments that melt only partially because of their attachment to other, higher melting parts of the crystalline matrix, the other is found for secondary, fringed-micellar crystals, grown

within the network of the primary crystals. In both cases, the amount of material and its local equilibrium melting temperature can be extracted from the DSTMC data.

Taking the data at 299 K listed in the discussion of Fig. 24, the modulation of 1.0 K adds a latent heat contribution to the true heat capacity of the semicrystalline sample of about $0.28\,J\,K^{-1}\,g^{-1}$ (the C_p of the melt is decreased by $0.06\,J\,K^{-1}\,g^{-1}$ for the existing 10% crystallinity). This latent heat involves a crystallinity change of $0.28\,J\,K^{-1}\,g^{-1} \times 1.0\,K \times 14.03\,g\,mol^{-1} \times 100/4110\,J\,mol^{-1} = 0.10\%$. Secondary, fringed-micellar crystals of this amount can easily be accommodated in the melting curves of the samples. Assuming further, that all of the about 10% crystals of the analyzed samples show such reversible crystallization and melting on their surfaces and that these crystals are isometric with a dimension of 5.0 nm, only ca. 1.5% of a monomolecularly occupied surface layer of 0.5 nm thickness need be involved in the reversible melting and crystallization to account for the higher apparent heat capacity. If this were one single molecular segment on each of the four growth faces of the assumed crystal, it would have a molar mass of the proper magnitude to melt and crystallize at 299 K, namely, 282 Da ($\approx C_{20}H_{40}$). Both estimates show that in such a metastable, poorly-crystallized sample it is possible to have local equilibria that are not restricted by molecular nucleation.

6. Conclusions

With the developments of DSTMC analyses described in Section 4 of this paper one can cover with present day DSC equipment times from about 10 to 1000 s. It is likely that extensions to time scales from 1 to 10,000 s can be achieved with the next generation of DSC equipment, i.e. four of the 18 orders of magnitude of time involved in the discussion of calorimetry can be measured directly. Times as short as 2×10^{-5} s can be measured with ac calorimetry, discussed elsewhere in this issue. The jump to picoseconds (10^{-12} s) is possible by fitting heat capacities to quantum-mechanical models for the change of heat capacity with temperature, as discussed in Sections 2 and 3 of this paper. Finally, long term experiments as one finds in crystal rearrangement may easily extended to megaseconds (10^6 s), as illustrated in Section 5 of this review.

Acknowledgements

This work was supported by the Division of Materials Research, National Science Foundation, Polymers Program, Grant No. DMR-9703692 and the Division of Materials Sciences and Engineering, Office of Basic Energy Sciences, U.S. Department of Energy at Oak Ridge National Laboratory, managed and operated by UT-Batelle, LLC, for the U.S. Department of Energy, under contract number DOE-AC05-00OR22725.

References

[1] M. Reading, Trends Polym. Sci. 8 (1993) 248.
[2] M. Reading, D. Elliot, V.L. Hill, J. Thermal Anal. 40 (1993) 949.
[3] P.H. Gill, S.R. Sauerbrunn, M. Reading, J. Thermal Anal. 40 (1993) 931.
[4] B. Wunderlich, Y. Jin, A. Boller, Thermochim. Acta 238 (1994) 277.
[5] A. Boller, Y. Jin, B. Wunderlich, J. Thermal Anal. 42 (1994) 307.
[6] Thermochim. Acta 304/305 (1997).
[7] Thermochim. Acta 330 (1999).
[8] Thermochim. Acta, this issue.
[9] B. Wunderlich, A. Boller, I. Okazaki, K. Ishikiriyama, Thermochim. Acta 304/305 (1997) 125.
[10] B. Wunderlich, A. Boller, I. Okazaki, K. Ishikiriyama, W. Chen, M. Pyda, J. Pak, I. Moon, R. Androsch, Thermochim. Acta 330 (1999) 21.
[11] A. Boller, C. Schick, B. Wunderlich, Thermochim. Acta 266 (1995) 97.
[12] B. Wunderlich, A. Boller, I. Okazaki, S. Kreitmeier, J. Thermal Anal. 47 (1996) 1013.
[13] I. Okazaki, B. Wunderlich, J. Polym. Sci. Part B: Polym. Phys. 34 (1996) 2941.
[14] L.C. Thomas, A. Boller, I. Okazaki, B. Wunderlich, Thermochim. Acta 291 (1997) 85.
[15] I. Okazaki, B. Wunderlich, Macromolecules 30 (1997) 1758.
[16] I. Okazaki, B. Wunderlich, Macromol. Chem. Phys. Rapid Commun. 18 (1997) 313.
[17] K. Ishikiriyama, B. Wunderlich, Macromolecules 30 (1997) 4126.
[18] K. Ishikiriyama, B. Wunderlich, J. Polym. Sci. Part B, Polym. Phys. 35 (1997) 1877.
[19] B. Wunderlich, Macromolecular Physics, Vol. 3, Crystal Melting, Academic Press, New York, 1980.

[20] R. Androsch, B. Wunderlich, Macromolecules 32 (1999) 7238.
[21] R. Androsch, B. Wunderlich, Macromolecules 33 (2000) 9076.
[22] B. Wunderlich, R. Androsch, M. Pyda, Y.K. Kwon, Thermochim. Acta 348 (2000) 181.
[23] M. Pyda, M., Y.K. Kwon, B. Wunderlich, Thermochim. Acta 367/368 (2001) 217.
[24] J. Pak, B. Wunderlich, Thermochim. Acta 367/368 (2001) 229.
[25] Y.K. Kwon, R. Androsch, M. Pyda, B. Wunderlich, Thermochim. Acta 367/368 (2001) 203.
[26] B.G. Sumpter, D.W. Noid, G.L. Liang, B. Wunderlich, Atomistic Dyn. Macromol. Crystals, Adv. Polym. Sci. 116 (1994) 27.
[27] S.N. Kreitmeier, G.L. Liang, D.W. Noid, B.G. Sumpter, Thermochim. Acta 46 (1996) 871.
[28] B. Wunderlich, Thermochim. Acta 300 (1997) 43.
[29] B. Wunderlich, Pure Appl. Chem. 67 (1995) 1919, for data and further information, see also the web-site: http://web.utk.edu/~athas.
[30] A.T. Petit, P.L. Dulong, Ann. Chim. Phys. 10 (1819) 395.
[31] A. Einstein, Ann. Phys. 22 (1907) 180, 800.
[32] P. Debye, Ann. Phys. 39 (1912) 789.
[33] M. Blackman, The specific heat of solids, in: S. Flügge (Ed.), Encyclopedia of Physics, Vol. VII, Part 1, Springer, Berlin, 1955.
[34] W. Nernst, F.A. Lindemann, Z. Electrochem. 17 (1911) 817.
[35] R. Pan, M. Varma, B. Wunderlich, J. Thermal Anal. 35 (1989) 955.
[36] Y. Kim, H.L. Strauss, R.G. Snyder, J. Chem. Phys. 93 (1989) 7520.
[37] B. Wunderlich, J. Polym. Sci., Part C 1 (1963) 41.
[38] B. Wunderlich, M. Möller, J. Grebowicz, H. Baur, Conformational Motion and Disorder in Low and High Molecular Mass Crystals, Springer, Berlin, 1988 (Adv. Polym. Sci., Vol. 87).
[39] G. Herzberg, Molecular Spectra and Molecular Structure, II. Infrared and Raman Spectra of Polyatomic Molecules, van Nostrand, Princeton, NJ, 1945.
[40] H. Baur, Colloid Polym. Sci. 252 (1974) 641.
[41] M. Pyda, B. Wunderlich, Macromolecules 32 (1999) 2044.
[42] W. Kauzmann, Chem. Rev. 43 (1948) 219.
[43] B. Wunderlich, Macromolecular Physics, Vol. 1, Crystal Structure, Mmorphology, Defects, Academic Press, New York, 1974.
[44] B. Wunderlich, Thermochim. Acta 355 (2000) 43.
[45] R. Androsch, M. Pyda, H. Wang, B. Wunderlich, J. Thermal Anal. Calorim. 61 (2000) 661.
[46] R. Androsch, I. Moon, S. Kreitmeier, B. Wunderlich, Thermochim. Acta 357/358 (2000) 267.
[47] I. Moon, R. Androsch, B. Wunderlich, Thermochim. Acta 357/358 (2000) 285.
[48] R. Androsch, J. Thermal Anal. Calorim. 61 (2000) 75.
[49] P. Kamasa, M. Pyda, M. Merzlyakov, J. Pak, C. Schick, B. Wunderlich, Thermochim. Acta, 2001, in press.
[50] A. Toda, T. Oda, M. Hikosaka, Y. Saruyama, Thermochim. Acta 293 (1997) 47.
[51] H. Hirai, H. Eyring, J. Appl. Phys. 12 (1958) 810.
[52] B. Wunderlich, D.M. Bodily, M.H. Kaplan, J. Appl. Phys. 35 (1964) 95.
[53] C. Schick, M. Merzlyakov, A. Hensel, J. Chem. Phys. 111 (1999) 2695.
[54] P. Kamasa, M. Pyda, M. Merzlyakov, C. Schick, B. Wunderlich, in: D.E. Jones (Ed.), Proceedings of the 28th NATAS Conference, Vol. 28, Orlando, FL, 4–6 October 2000, p. 889.
[55] K. Ishikiriyama, A. Boller, B. Wunderlich, J. Thermal Anal. Calorim. 50 (1997) 547.
[56] A. Wurm, M. Merzlyakov, C. Schick, J. Thermal Anal. Calorim. 60 (2000) 807.